



UNIVERSIDADE ESTADUAL DE CAMPINAS
SISTEMA DE BIBLIOTECAS DA UNICAMP
REPOSITÓRIO DA PRODUÇÃO CIENTÍFICA E INTELLECTUAL DA UNICAMP

Versão do arquivo anexado / Version of attached file:

Versão do Editor / Published Version

Mais informações no site da editora / Further information on publisher's website:

<https://pubs.rsc.org/en/content/articlelanding/2014/TA/c3ta12892j>

DOI: 10.1039/c3ta12892j

Direitos autorais / Publisher's copyright statement:

©2014 by Royal Society of Chemistry. All rights reserved.

DIRETORIA DE TRATAMENTO DA INFORMAÇÃO

Cidade Universitária Zeferino Vaz Barão Geraldo

CEP 13083-970 – Campinas SP

Fone: (19) 3521-6493

<http://www.repositorio.unicamp.br>

Designing nanoscaled hybrids from atomic layered boron nitride with silver nanoparticle deposition†

Cite this: *J. Mater. Chem. A*, 2014, 2, 3148

Guanhui Gao,^{ab} Akshay Mathkar,^b Eric Perim Martins,^c Douglas S. Galvão,^c Duyang Gao,^a Pedro Alves da Silva Autreto,^c Chengjun Sun,^{*d} Lintao Cai^{*a} and Pulickel M. Ajayan^{*b}

We have developed a microwave assisted one-pot approach to fabricate a novel hybrid nano-composite composed of two-dimensional chemically exfoliated layered hexagonal boron nitride (h-BN) and embedded silver nanoparticles (SNP). Atomic layered h-BN exfoliated using chemical liquid showed strong in-plane bonding and weak van der Waals interplanar interactions, which is utilized for chemically interfacing SNP, indicating their ability to act as excellent nano-scaffolds. The SNP/h-BN optical response, in particular band gap, is strongly dependent on the concentration of the metallic particles. In order to gain further insight into this behavior we have also carried out *ab initio* density functional theory (DFT) calculations on modeled structures, demonstrating that the bandgap value of SNP/h-BN hybrids could be significantly altered by a small percentage of OH⁻ groups located at dangling B and N atoms. Our results showed that these novel SNP/h-BN nanohybrid structures exhibited excellent thermal stability and they are expected to be applied as devices for thermal oxidation-resistant surface enhanced Raman spectroscopy (SERS). The SNP/h-BN membrane showed remarkable antibacterial activity, suggesting their potential use in water disinfection and food packaging.

Received 25th July 2013
Accepted 14th November 2013

DOI: 10.1039/c3ta12892j

www.rsc.org/MaterialsA

Introduction

Silver nanoparticles (SNP) and silver-based compounds have received an enormous amount of attention due to their unique optical, electrochemical, catalytical, and bactericidal properties;¹⁻⁴ moreover, their highly antiseptic property is especially attractive because of the low toxicity of active silver ions to human cells.^{5,6} Various techniques have been developed to synthesize SNP containing composite materials, such as carbon nanotubes (CNTs), silicon dioxide, titanium dioxide, and graphene oxide (GO).⁷⁻¹⁰ The general strategy for fabricating these “nanohybrids” involves chemical reduction of the silver precursors, followed by either reaction or adsorption inside the desired scaffold to form a stable composite. Recent efforts have focused on loading SNP onto two-dimensional materials to increase the accessible surface area. For instance, efficient

synthesis strategies of SNP/GO nanohybrids have been reported by a number of studies ranging in applications from hydrogen peroxide (H₂O₂) detection to efficient bactericidal agents.¹¹⁻¹³

Isostructural to graphene, hexagonal boron nitride (h-BN) sheet is another atomic-thick two dimensional material possessing a highly diverse set of properties inconceivable from graphene: such as large bandgap and outstanding chemical and thermal stability. Its pronounced thermal oxidation-resistant property makes it a superior scaffolding candidate for certain chemically hazardous applications.¹⁴⁻¹⁶ However, h-BN has been challenging due to its exceptional intersheet-bonding and chemical inertness. To develop applications of the h-BN monolayer, our previous report demonstrated layer-by-layer exfoliation of h-BN nanosheet based chemical liquid treatment with high yields.¹⁷ This also led to the transformation of the chemically passive BN lattice to its chemically active form enabling its interfacing with noble metal nanoparticles.

In this study, we report a novel, microwave assisted one-pot approach to synthesize hybrid composites consisting of SNP deposited onto exfoliated h-BN sheets in dimethylformamide (DMF), with the solvent DMF acting as both the reducing agent¹⁸ and the chemical liquid for exfoliation of layered h-BN nanosheets, because DMF is known to be a good dispersant for h-BN and graphene exfoliation.¹⁷ Loading of SNP on h-BN nanosheets was found to affect the optical band gap (E_g), which can be easily tuned by controlling the SNP concentration. This suggests a strong interaction between SNP and the layered h-BN

^aGuangdong Key Laboratory of Nanomedicine, Institute of Biomedicine and Biotechnology, Shenzhen Institutes of Advanced Technology, Chinese Academy of Sciences, Shenzhen 518055, P.R. China. E-mail: lt.cai@siat.ac.cn

^bDepartment of Mechanical Engineering & Materials Science, Rice University, Houston, Texas 77005, USA. E-mail: ajayan@rice.edu

^cApplied Physics Department, State University of Campinas, 13083-959 Campinas, SP, Brazil

^dMarine Ecology Center, the First Institute of Oceanography, SOA, Qingdao, P.R. China. E-mail: csun@fio.org.cn

† Electronic supplementary information (ESI) available. See DOI: 10.1039/c3ta12892j

nanosheets. Simulations *via* the Dmol3 method were conducted in order to further investigate the van der Waals interactions between the faceted shape of SNP deposited onto layered h-BN nanosheets, and the reason leading to the bandgap of SNP/h-BN hybrids varied with different amounts of the aqueous silver nitrate precursor.

Experimental section

Materials

Boron nitride powder ($\sim 1 \mu\text{m}$, 98%), silver nitrate (AgNO_3 , $\geq 99.8\%$), and DMF were all purchased from Sigma Aldrich and used as supplied.

Preparation of exfoliated h-BN nanosheets and SNP/h-BN composites

We sonicated boron nitride powder (100 ml cylindrical vial, starting concentration 1.0 mg ml^{-1}) in a low power sonic bath for 2 hours. This resulted in milky white dispersions of h-BN. The resultant dispersion was centrifuged at 1500–4000 rpm for 30 minutes. The supernatant (top two thirds of the centrifuged dispersion) was collected by pipetting. We adopted the protocols from our previous work on graphene exfoliation.¹⁵ After centrifugation, the exfoliated h-BN supernatant was filtered using a polytetrafluoroethylene (PTFE) membrane ($0.2 \mu\text{m}$ pore size, 47 diameter, Millipore) and dried in order to calculate the yield of h-BN exfoliation (ESI, Fig. S1[†]).

Different volumes of 10^{-2} M AgNO_3 (in order to investigate the loading capacity of SNP to h-BN layers) aqueous solutions were added into the exfoliated h-BN/DMF (5 mg/5 ml) mixture respectively and sonicated for 15 minutes, followed by microwave assisted irradiation for 2–10 seconds to accelerate the growth of metallic nanoparticles. The grown silver nanoparticles embedded in atomic layered h-BN nanosheets forming SNP/h-BN hybrid composites. The color of the solution changed from colorless to light yellow, red and brownish with different amounts of AgNO_3 added, indicating the nucleation of the silver particles at their infancy (ESI, Fig. S2[†]).

Analysis and instruments

Transmission electron microscopy (TEM) analyses were carried out with a JEOL-2010, LaB₆ operated at 100 kV. High-resolution TEM images were taken with the JEOL-2100F, operated at

200 kV. Electron energy-loss spectroscopy (EELS) and energy-dispersive X-ray spectroscopy (EDS) measurements were carried out on the JEOL-2100 field emission HRTEM operated at 200 kV. XPS (PHI Quantera XPS) was carried out using monochromatic aluminium $K\alpha$ X-rays. XPS data were analyzed with the MultiPak software. Raman spectroscopy was used to characterize the structure of the film at 514 nm laser excitation. Optical-absorptance measurements (Shimadzu ultraviolet-3600) were performed using 1 cm quartz. X-ray diffraction (XRD) with Rigaku D/Max Ultima II Powder XRD configured with a vertical theta/theta goniometer, Cu $K\alpha$ radiation, graphite monochromator, and scintillation counter. The microwave reaction was conducted with WF-4000 (heat temperature: 0–250 °C, stirring speed: 1000 rpm). The thermal stability of SNP and SNP/h-BN hybrid dispersed in water was measured by dynamic light scattering (DLS), using a Malvern ZetaSizer (NanoZS).

Results and discussion

We successfully created a one-pot approach to synthesize SNP/h-BN nanohybrids in which DMF played dual roles as both the exfoliation solvent and reducing agent (Fig. 1). Exfoliated h-BN dissolved in a solution of DMF and silver nitrate was added dropwise. The synthesis of SNP/h-BN nanohybrid suspension without any aggregation was achieved through microwave assisted treatment which played a role in accelerating the uniform growth of silver nanoparticles 5–10 nm in diameter without any surfactants. Seconds after microwave irradiation, the solution changed from milky to dark brown color indicating the formation of silver nanoparticles (ESI, Fig. S2[†]). The advantage of the microwave-assisted reduction is that it requires much less time due to localized heat at reaction sites. This makes our facile method a better candidate toward large-scale processing.

The morphology of the synthesized nanohybrids was analyzed using low-resolution TEM (Fig. 2a and b and ESI, Fig. S3[†]). The images showed even dispersion of SNP throughout the h-BN sheets, with no signs of aggregation. The h-BN nanosheets served as templates for subsequent growth of silver nanoparticles on their surface. In particular, a large number of SNP seemed to embed in the edges of the h-BN sheets. This could be attributed to the sp^2 hybridization of h-BN, which made the edges more chemically active to attract

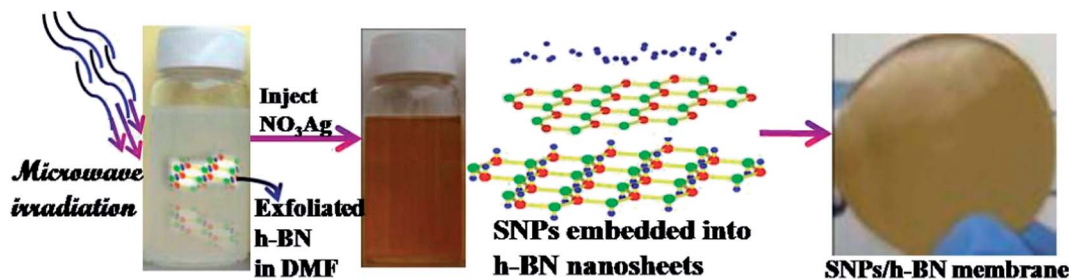


Fig. 1 Schematic synthesis process of SNP/h-BN nanohybrids *via* a microwave-assisted method. Exfoliated h-BN dissolved in DMF with silver nitrate solution results in the fabrication of SNP/h-BN nanohybrid suspension without any aggregation phenomenon.

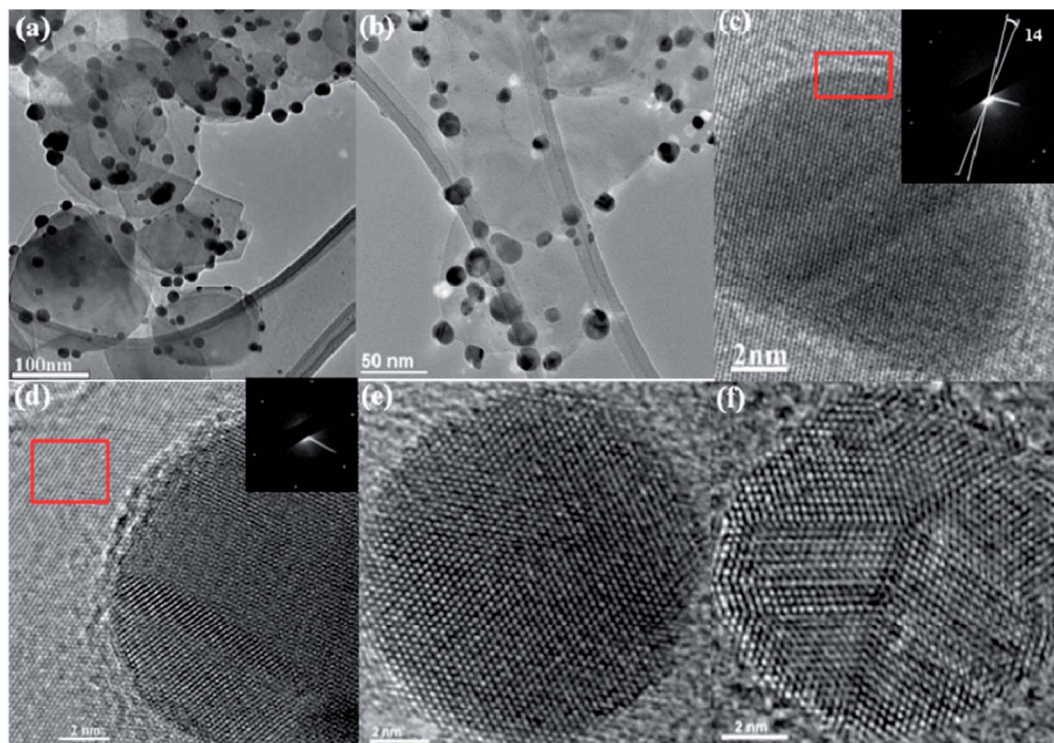


Fig. 2 Typical TEM images of SNP/h-BN hybrid composites: (a and b) low-resolution TEM; (c) high-resolution TEM polycrystalline silver nanoparticles, the FFT in the inset reveals the edge of silver nanoparticles stacked onto h-BN with a relative rotational angle of 14° (red line area); (d) high-resolution TEM polycrystalline silver nanoparticles, the FFT in the inset of a single layered hexagonal lattice of boron nitride nanosheets (red line area); (e) single crystalline structural silver nanoparticles; and (f) multi-crystalline structural silver nanoparticles.

molecules or atoms. Specifically, the binding energy decreased around the edge area, which was available for coalescing silver nanoparticles maintaining chemical stability. High-resolution TEM (HRTEM) analysis confirmed that the size distribution of SNP was between 5 and 10 nm. Fast Fourier transform (FFT) spectrum of the zoom area in a red line displayed a relative rotational angle of 14° (the inset of Fig. 2c). This indicated a hexagonal structure between crystalline SNP and h-BN, while the inset of Fig. 2d showed a FFT pattern confirming the clear hexagonal lattice structure of layered h-BN. A closer look at the silver nanoparticles revealed their existence in both single crystalline lattice and twinned polyhedral states, as seen in Fig. 2e and f. Obviously, the defined morphology of the nano-hybrids confirmed that microwave radiation did not have adverse effects on the chemical structure such as sheet crumpling and dissociation, which tended to be issues during reduction involving other scaffolding materials.¹³

Electron energy loss spectroscopy (EELS) and energy dispersive X-ray spectroscopy (EDS) were used to identify the atomic composition. The dark-field image from EELS (Fig. 3a) and the corresponding K-shell edge (Fig. 3d) depicted the characteristic K-shell ionized edges of B and N with a typical peak of valence band edge π^* and conduction band σ^* at 190.5 eV and 407.6 eV (ref. 18–20) respectively. A weak peak of metallic Ag 3d, a value of 369.3 eV,²¹ was also present. The visible edges of B, N and Ag 3d revealed the existence of single or multi-layered h-BN and metallic Ag. Since the energy loss of Ag

was not sensitive under EELS measurement, we further investigated the atomic composition by EDS (Fig. 3b and c). The Ag peaks were apparent from Fig. 3c, corresponding to Ag 3d_{5/2} and Ag 3d_{3/2}, indicating the presence of Ag.

In order to probe the formation mechanism of SNP/h-BN nano-hybrids, we investigated the interaction between Ag atoms and B, N atoms using XPS. XPS spectra of SNP/h-BN composites showed the B 1s, N 1s core levels, and Ag 3d (Fig. 4(a–c) and ESI, Fig. S4†). The elemental scan of Ag 3d_{5/2} and Ag 3d_{3/2} core level peaks was centered at 367.1 eV and 373.0 eV respectively (Fig. 4c). This can be attributed to the valence state of Ag⁰ species suggesting that Ag⁺ ions from the solution have been reduced by DMF. Compared with the reported values of Ag 3d_{5/2} (367.9 eV) and Ag 3d_{3/2} (373.9 eV),²² both peaks observed shifted to lower binding energies by 0.8 eV and 0.9 eV respectively, indicating that the silver nanoparticles were loaded mainly on the surface of the h-BN substrate by either physical adsorption or electrostatic adsorption.^{23,24} The probable reaction mechanism for the synthesis of SNP/h-BN nano-hybrids was that when dropping aqueous silver nitrate solution into the h-BN/DMF mixture, and assisted by microwave irradiation, hydrolysis was triggered and the amount of hydroxyl groups located at dangling B, N atoms increased. This resulted in the adsorption of positive charges present on the surface of the silver nanoparticles as reported.¹⁸

Raman spectroscopy was performed with 514.5 nm laser excitation. A pristine h-BN signal peak is shown in Fig. 4d,

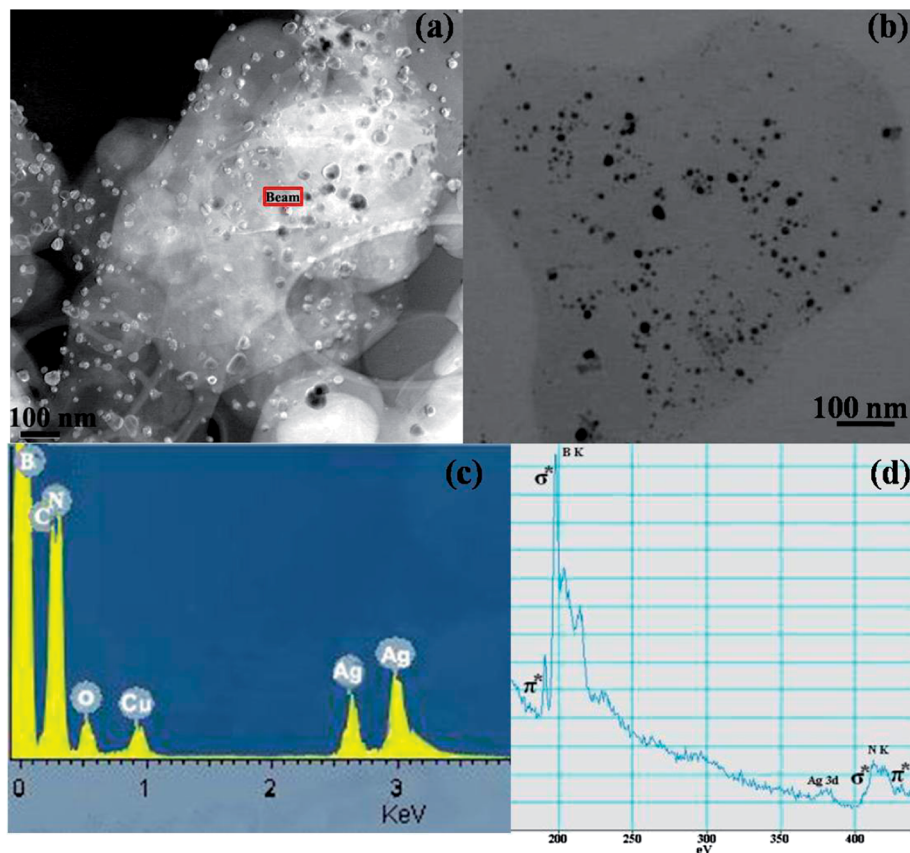


Fig. 3 The characterization for SNP/h-BN composites: (a) dark-field image from electron energy loss spectroscopy; (b) dark-field image from energy-dispersive X-ray spectrum; (c) energy-dispersive X-ray spectrum (EDX); (d) electron energy loss spectroscopy (EELS).

exhibiting the high-frequency E_{2g} intralayer phonon mode; the Raman line was located at 1365 cm^{-1} , and is consistent with values reported by other literature.¹⁵ However, there were several peaks besides the original h-BN peak in the SNP/h-BN composites, while the intensity decreased correspondingly. The Raman line has been shown to vary probably due to silver nanoparticle intercalation. When silver atoms occupied the random defect sites within the h-BN lattice, the van der Waals interactions and bandgap would change, resulting in the Raman lattice mode for in-plane motion (basal-plane dimension) reflecting the response of the interfaces between the B-N bond and atomic silver.^{25–27} More evidence of their binding mechanisms needs to be further exploited.

The XRD spectra indicated that the sharp and highest peak at 26.76° was from pure h-BN corresponding to (002) in SNP/h-BN composites (Fig. 4e). The facets of Ag crystal peaks were indexed as the (101), (111), (200), (220), (311), and (222) planes of cubic silver, which indicated the incorporation of Ag atoms.

The ultraviolet-visible absorption spectrum showed that the absorption peaks varied with different concentrations of silver nanoparticles deposited on layered h-BN leading to tunable band gap values. We estimated these values using Tauc's formula^{15,28} shown in Fig. 5b and S2† for the detailed calculations. We estimated the value for pure exfoliated h-BN nanosheets by measuring the UV-vis-IR absorption spectrum (Fig. 5a). The

absorption edge of exfoliated h-BN was located at 236 nm, which corresponded to an optical bandgap of 5.26 eV. Comparably, the absorption peaks of SNP/h-BN nanohybrids were located at 283 nm and 410 nm corresponding to pure h-BN and Ag interactions respectively by varying the volume ratio (ESI, Fig. S5†). This phenomenon proved that the band gap of h-BN could be varied with the number of silver nanoparticles deposited.^{29,30}

We subsequently addressed the bandgap behavior as a function of the amount of SNP. All bandgap calculations were carried out *via* the Dmol3 method as implemented on the Accelrys Materials Studio suite, using GGA functions under the PBE approximation. One possible explanation was that these changes were due to interlayer spacing changes induced by the presence of intercalated SNP. In Fig. 6 we showed the bandgap values as a function of the supercell interlayer distances. There was a small variation of less than 1 eV, which was too small to explain the bandgap change observed. So the bandgap changes must be attributed to another reason. Another possibility was related to OH and/or OH⁻ groups bonded to h-BN structures. We have considered a BN supercell containing 4 B and 4 N atoms. When one OH was added to the structure, if it is bonded to the B atom, the bandgap value would change from 4.7 eV to 4.9 eV, while no chemical bond was formed between OH and the N atom (basically only physisorption occurred) and the bandgap remained almost the same (from 4.71 eV to 4.73 eV).

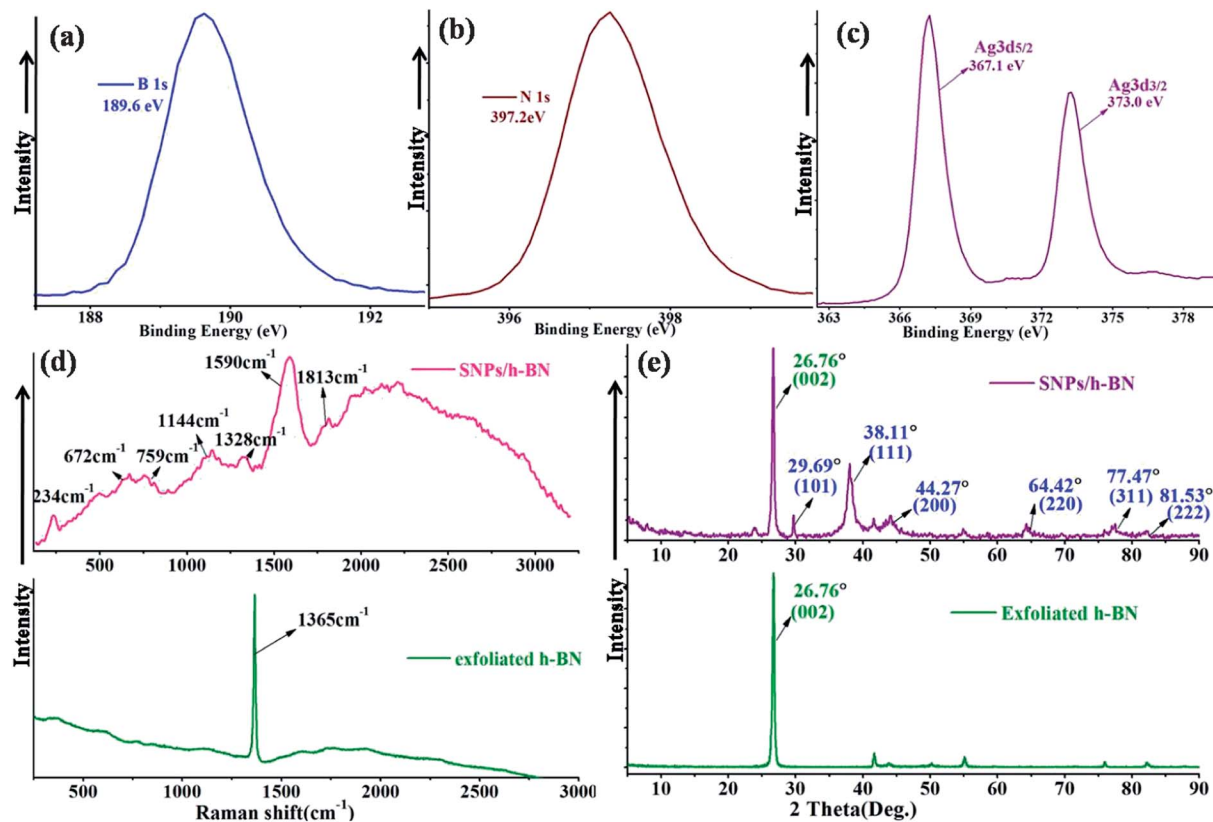


Fig. 4 (a–c) XPS spectra of B 1s, N 1s core levels and Ag 3d_{5/2}, Ag 3d_{3/2} in SNP/h-BN composites; (d) Raman spectra of exfoliated hexagonal boron nitride nanosheets and SNP/h-BN composites; (e) X-ray diffraction pattern of hexagonal BN nanosheets and SNP/h-BN composites.

These small changes were not consistent with the experimental data. However, when the presence of OH⁻ groups was considered, significant changes in the bandgap values were observed. When one OH⁻ group was bonded to a B atom, the bandgap value decreased from 4.7 eV to 4.2 eV. When the OH⁻ was brought close to a N atom, a chemical bond was now formed and the bandgap value went to 3.2 eV. Doubling the number of OH⁻ groups led to the bandgap value of 2.8 eV. When the OH⁻ groups were bonded only to N atoms, the

bandgap values were observed as small as 2.3 eV. Therefore, the observed behavior of the bandgap was considered to be a consequence of the presence of OH⁻ groups stabilized by the SNP and not the result of a direct interaction between the SNP and h-BN layers. Further studies are necessary to confirm this hypothesis.

The antibacterial activity of SNP/h-BN composites was investigated by plate counting and the inhibition zone method^{31–34} (ESI, Fig. S3† for the details on antibacterial measurement). A

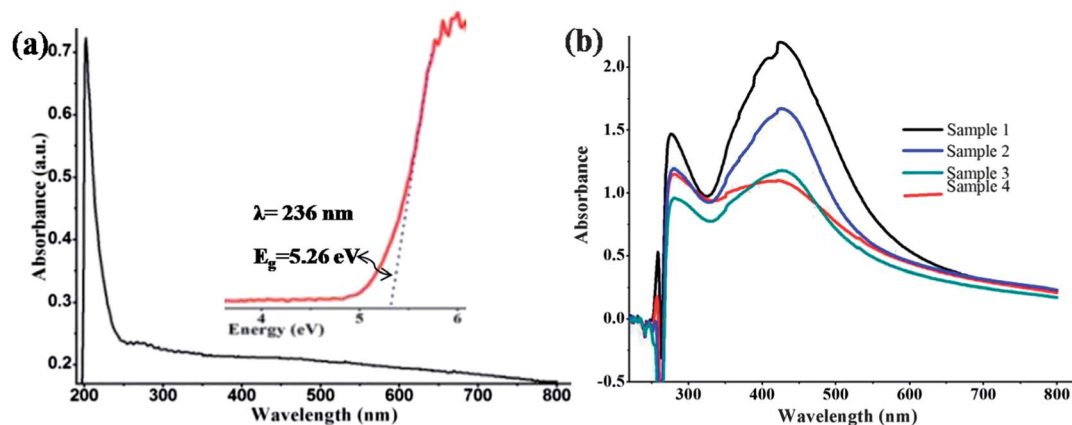


Fig. 5 (a) Ultraviolet-visible absorption spectrum of pure exfoliated h-BN, the inset shows the corresponding plot of $\epsilon_{1/2}/\lambda$ versus $1/\lambda$ by Tauc's formula calculation; (b) ultraviolet and visible spectroscopy of SNP/h-BN composites; sample 1: SNP/h-BN (wt 1.7/5); sample 2: SNP/h-BN (wt 2.55/5); sample 3: SNP/h-BN (wt 3.4/1); sample 4: SNP/h-BN (wt 4.25/5).

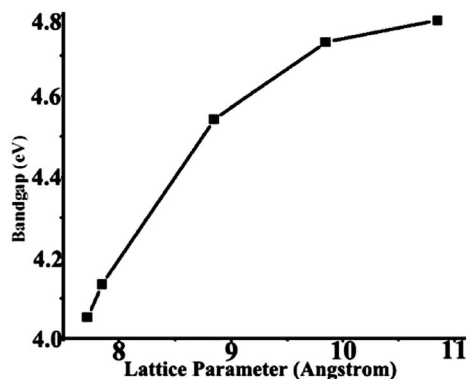


Fig. 6 Simulation of bandgap variation as a function of the supercell interlayer distances.

small inhibition zone was observed in the pure exfoliated h-BN membrane which provided evidence that h-BN had bactericidal properties (Fig. 7a). The antibacterial effect of SNP/h-BN composites was seen easily by adding different quantities of silver nanoparticles. The results illustrated that the diameter of the inhibition zone was enlarged by increasing the concentration of silver nanoparticles (Fig. 7b–f), which demonstrated that SNP/h-BN composites possessed a more pronounced antibacterial property. For comparison, the same volume of a pure silver nanoparticle sample was investigated; we obtained similar phenomena of inhibition, but the antibacterial durability effect of SNP/h-BN hybrids was much better than pure SNP due to oxidation. Furthermore, thermal stability tests indicated that the SNP/h-BN hybrid was stable up to 85 °C, which was superior to

that of pure SNP (ESI, Fig. S7†). Notably, the SNP/h-BN composite membranes prepared after filtration possessed an interesting hydrophobic property for promising water disinfection films. The excellent antimicrobial effect of the SNP/h-BN nanohybrid film was preserved at room temperature under ambient conditions for 6 months, which exhibited its long-term stability.

Conclusion

In conclusion, we reported the synthesis of new hybrid nanocomposites composed of silver nanoparticles deposited onto hexagonal boron nitride layers by a one-pot microwave assisted procedure. The chemical exfoliation technique used here resulted in random single or double layer nanosheets serving as substrates for SNP. The fabrication mechanism of SNP/h-BN nanohybrids occurred mainly by physical adsorption and electrostatic interaction. Simulation results illustrated that faceted shape SNP affected the van der Waals interactions of layered h-BN nanosheets. The interplanar spacing of layered h-BN changed due to embedded SNP, but the reason that led to the variation of the bandgap of SNP/h-BN hybrids should be attributed to a small amount of hydroxyl groups located at dangling B and N atoms. Notably, these hybrid nano-composites show excellent thermal stability, and remarkable antibacterial activity, suggesting their potential use in water disinfection and purification.

Acknowledgements

This research was supported by the Science and technology innovation fund of Shenzhen (JCYJ20130401170306832);

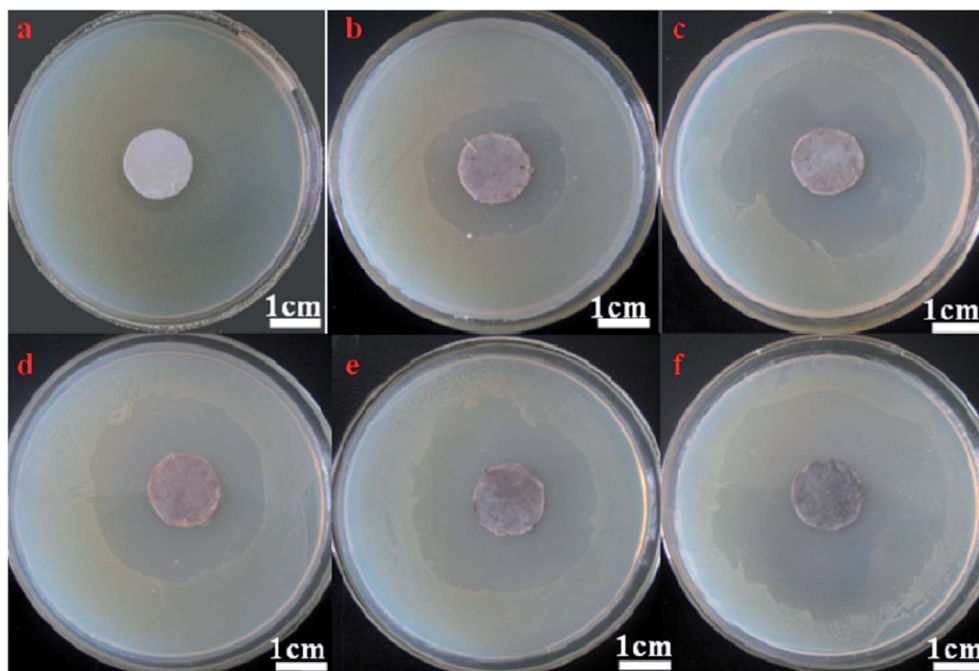


Fig. 7 The antibacterial effects of SNP/h-BN composites by inhibition zone measurement: (a) the control sample of *Chlorophenols arthrobacter* (C.A) bacteria growing on the pure h-BN membrane; (b) SNP/h-BN composites (0.17/5, wt); (c) SNP/h-BN composites (0.85/5, wt); (d) SNP/h-BN composites (1.7/5, wt); (e) SNP/h-BN composites (2.55/5, wt); (f) SNP/h-BN composites (3.4/5, wt).

National Natural Science Foundation of China (grant no. 31100567); start-up grant from the First Institute of Oceanography (GY02-2011T10) and the MOHRSS (Ministry of Human Resources and Social Security of China), Taishan Scholar Fund, and the National Natural Science Foundation of China (grant no. 81071249, 81171446, 20905050, and 61205203). Douglas S. Galvao, Pedro A. S. Autreto and Eric Perim acknowledge partial support from the Brazilian agencies CNPq and Fapesp.

References

- 1 K. S. Subrahmanyam, A. K. Manna, S. K. Pati and C. N. Rao, *Chem. Phys. Lett.*, 2010, **497**, 70–75.
- 2 R. R. Naik, S. J. Stringer and G. Agarwal, *Nat. Mater.*, 2002, **1**(3), 169–172.
- 3 C. P. Chen, P. Gunawan, X. W. Lou and R. Xu, *Adv. Funct. Mater.*, 2012, **22**, 780–787.
- 4 H. Arnim, *Chem. Rev.*, 1989, **89**(8), 1861–1873.
- 5 A. Kameo, T. Yoshimura and K. Esumi, *Colloids Surf., A*, 2003, **215**, 181–189.
- 6 L. K. Braydich-Stolle, B. Lucas, A. Schrand, R. C. Murdock, T. Lee, J. J. Schlar, S. M. Hussain and M. C. Hofmann, *Toxicol. Sci.*, 2010, **116**(2), 577–589.
- 7 S. Liu, L. Wang, J. Tian, Y. Luo, X. Zhang and X. Sun, *J. Colloid Interface Sci.*, 2011, **363**, 615–619.
- 8 J. X. Wang, L. X. Wen, Z. H. Wang and J. F. Chen, *Mater. Chem. Phys.*, 2006, **96**, 90–97.
- 9 G. Gao, Y. Lei, L. Dong, W. Liu, X. Wang, X. Chang, T. Liu and Y. Yin, *Mater. Express*, 2012, **2**(2), 1–9.
- 10 T. Hirakawa and P. V. Kamat, *J. Am. Chem. Soc.*, 2005, **127**(11), 3928–3934.
- 11 S. Liu, J. Tian, L. Wang and X. Sun, *J. Nanopart. Res.*, 2011, **13**(10), 4539–4548.
- 12 S. W. Chook, C. H. Chia, S. Zakaria, M. K. Ayob, K. L. Chee, H. M. Neoh and N. M. Huang, *Adv. Mater. Res.*, 2012, **364**, 439–443.
- 13 Q. Bao, D. Zhang and P. Qi, *J. Colloid Interface Sci.*, 2011, **360**, 463–470.
- 14 L. Ci, L. Song, C. Jin, D. Jariwala, D. Wu, Y. Li, A. Srivastava, Z. F. Wang, K. Storr, L. Balicas, F. Liu and P. M. Ajayan, *Nat. Mater.*, 2010, **9**, 430–435.
- 15 L. Song, L. Ci, H. Lu, P. B. Sorokin, C. Jin, J. Ni, A. G. Kvashnin, D. G. Kvashnin, J. Lou, B. I. Yakobson and P. M. Ajayan, *Nano Lett.*, 2010, **10**, 3209–3215.
- 16 Z. Liu, L. Song, S. Zhao, J. Huang, L. Ma, J. Zhang, J. Lou and P. M. Ajayan, *Nano Lett.*, 2011, **11**(5), 2032–2037.
- 17 G. Gao, W. Gao, J. Taha, L. Balicas, A. Mathkar, T. N. Narayanan, Z. Liu, B. K. Gupta, J. Peng, Y. Yin, A. Rubio and P. M. Ajayan, *Nano Lett.*, 2012, **12**(7), 3518–3525.
- 18 I. Pastoriza-Santos and L. M. Liz-Marzán, Reduction of silver nanoparticles in DMF. Formation of monolayers and stable colloids, *Pure Appl. Chem.*, 2000, **72**(1–2), 83–90.
- 19 Y. Lin, T. V. Williams, T.-B. Xu, W. Cao, H. E. Elsayed-Ali and J. W. Connell, *J. Phys. Chem. C*, 2011, **115**, 2679–2685.
- 20 J. C. Meyer, A. Chuvilin, G. Algara-Siller, J. Biskupek and U. Kaiser, *Nano Lett.*, 2009, **9**, 2683–2689.
- 21 N. Alem, R. Erni, C. Kisielowski, M. D. Rossell, W. Gannett and A. Zettl, *Phys. Rev. B: Condens. Matter Mater. Phys.*, 2009, **80**, 155425.
- 22 R. Arenal, M. Kociak and N. J. Zaluzec, *Appl. Phys. Lett.*, 2007, **90**, 204105.
- 23 R. R. Naik, S. J. Stringer, G. Agarwal, S. E. Jones and M. O. Stone, *Nat. Mater.*, 2002, **1**(3), 169–172.
- 24 Y. Miyamoto, A. Rubio, S. G. Louie and M. L. Cohen, *Phys. Rev. B: Condens. Matter Mater. Phys.*, 1994, **50**, 18360.
- 25 R. Geick and C. H. Perry, *Phys. Rev.*, 1966, **146**, 543–547.
- 26 G. L. Doli, J. S. Speck, G. Dresselhaus and M. S. Dresselhaus, *J. Appl. Phys.*, 1989, **66**, 2554.
- 27 S. Panigrahi, S. Praharaj, S. Basu, S. K. Ghosh, S. Jana, S. Pande, T. Vo-Dinh, H. Jiang and T. Pal, *Phys. Chem. B*, 2006, **110**, 13436–13444.
- 28 T. Wu, H. Shen, L. Sun, B. Cheng, B. Liu and J. Shen, *ACS Appl. Mater. Interfaces*, 2012, **4**(4), 2041–2047.
- 29 Y. Lin, C. E. Bunker, K. A. Shiral Fernando and J. W. Connell, *ACS Appl. Mater. Interfaces*, 2012, **4**(2), 1110–1117.
- 30 Y. Zhang, X. Yuan, Y. Wang and Y. Chen, *J. Mater. Chem.*, 2012, **22**, 7245–7251.
- 31 A. Kumar, P. K. Vemula, P. M. Ajayan and G. John, *Nat. Mater.*, 2008, **7**, 236.
- 32 Q. L. Feng, J. Wu, G. Q. Chen, F. Z. Cui, T. N. Kim and J. O. Kim, *J. Biomed. Mater. Res.*, 2000, **52**, 662–668.
- 33 I. Ahmed, D. Ready, M. Wilson and J. C. Knowles, *J. Biomed. Mater. Res., Part A*, 2006, **79**, 618–626.
- 34 W. Yuan, G. Jiang, J. Che, X. Qi, R. Xu, M. W. Chang, Y. Chen, S. Y. Lim, J. Dai and M. B. Chan-Park, *J. Phys. Chem. C*, 2008, **112**, 18754–18759.